Full Energy Management of EO-AAC: Toward a Dynamic Equivalence with MMC

Full Energy Management of EO-AAC: Toward a Dynamic Equivalence with MMC

Pierre Vermeersch, Francois Gruson, *Member, IEEE* Michael M. C. Merlin, *Member, IEEE,* Xavier Guillaud, *Member, IEEE* and Philippe Egrot

***Abstract*—Energy management in modular type converters constitutes a key aspect of their operational stability. This paper introduces a full energy management structure for the Extended Overlap-Alternate Arm Converter (EO-AAC) ensuring both equal energy distribution across all six stacks and the maintaining of ripple-free DC current during steady state. The performance of the control structure against active power step events is validated by detailed simulations using EMTP-RV software. Moreover, the full energy management allows the EO-AAC to have an equivalent controllability to Modular Multilevel Converter (MMC) through only two conducting stacks in overlap mode ensuring the power balance. From this observation, it is demonstrated that the use of control strategy like the virtual capacitor to support HVDC system, originally designed for MMC, is possible.**

Gathering all these controllers leads to a general conclusion which is the dynamic equivalence between EO-AAC and MMC.

***Index Terms*—High Voltage Direct Current, Alternate Arm Converter, Energy Management, DC Voltage Control**

I. Introduction

OVER the last decade, modular type converters, essentially Modular Multilevel Converter (MMC), have been one of the main subject of interest for the potential future grid including more DC transmission system connected to the current AC system. Since the advent of the MMC in [1], whose operation is based on DC side stacked Sub-Modules (SMs), various topologies have been proposed with, for some of them, different stack arrangements [2]–[6]. The resulting topologies present, most of the time, some improvements over the reference topology that is the Half-Bridge (HB) MMC in terms of station footprint, reduced number of SMs, energy storage requirement, DC fault blocking capability [7], losses or even power capability [8]. However, these interesting improvements on converter physical parts often hide more complex internal mechanisms making modelling, control achievement and dynamic behaviour analysis really challenging, but essential for grid connected converters.

One of these topologies, is the Alternate Arm Converter, an hybrid topology combining features of the original 2-level VSC and the Full-Bridge (FB) MMC [7] as illustrated on Fig. 1. The converter arms consist in a serial connection of a stack of FB-SMs and a Director Switch (DS). The DS is composed of several fully controllable power devices [9] used to reduce arm conduction periods in a such way that the upper arm modulates the positive part of the AC voltage while the lower arm the negative part. These operations, allows the AAC to require less SMs and energy storage than the HB-MMC [10] while having the DC fault blocking capability and better efficiency than the FB-MMC [7], [11]. However, the original AAC suffers from a small voltage range of operation due to high energy balancing current [11], [12] and requires a bulky passive DC filter to compensate DC current harmonics resulting from the arm alternation.

Recently, the Extended Overlap-Alternate Arm Converter (EO-AAC) has been developed and presented in [11]. The EO-AAC extends the arm conduction period until both arms of a phase leg form a 60 degree overlap period, where a MMC-like operating mode is possible greatly improving the converter controllability. It results a converter able to operate with a wide range in terms of modulation ratio and to generate ripple free DC and AC currents. Thus, compared to the reference HB-MMC, the EO-AAC provides an equivalent energy quality, a more compact design [11] and the DC fault-capability. However, these interesting features are obtained at the expense of higher losses due to FB-SMs and more complex internal operations and control. Until now, the control of the EO-AAC and especially its energy management has only been partially investigated. The original paper of the EO-AAC provides explanations on the operating principles and experimental results while [13] and [14] present energy controllers leaving some of the energy dynamics uncontrolled. Thus, a complete control of the EO-AAC energy dynamics is still missing in the current literature. Unlike the conventional AAC or even the MMC, DC power-based energy control in EO-AAC is subject to two constraints. The first one, common to every modular converters, it must provide a full management of each stack energy while the second is the need of explicit DC current reference. Therefore, this paper provides a comprehensive analysis of energy inside EO-AAC to derive controls fulfilling these constraints. It is organised as follows: In section II the main principles of the EO-AAC are briefly presented to obtain expressions of electrical quantities required for analysing energy deviations inside stacks. Then, Section III analyses existing energy control techniques to highlight capabilities, limitations when considering the case of the EO-AAC. Section IV details the inter-legs stored energy control ensuring a full energy dynamics control inside the EO-AAC. Finally, Section V investigates the use of the EO-AAC internal energy to support HVDC system.

P. Vermeersch, F. Gruson and X. Guillaud are with Univ. Lille, Arts et Metiers Institute of Technology, Centrale Lille, Junia, ULR 2697 - L2EP, F-59000 Lille, France

M.M.C. Merlin is with School of Engineering, University of Edinburgh, Edinburgh, UK

P. Egrot is with Electricité de France R&D - EDF R&D, Moret-sur-Loing, France

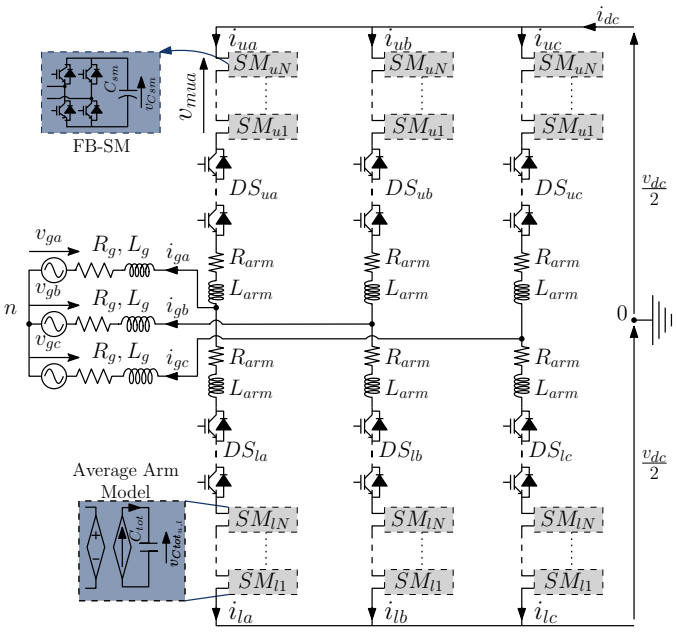

Fig. 1. Alternate Arm Converter scheme

II. Extended Overlap Alternate Arm Converter

To achieve energy analysis, arm voltage and current expressions are required. They depends on the arm operating modes. For the sake of simplicity, explaining the arm operations is best achieved by decomposing them in Non-overlap and Overlap modes illustrated on Fig. 3.

A. Non-overlap mode

During this operating mode, only one arm of a leg is conducting the grid current. Assuming the upper arm conducting gives:

$$\begin{cases} i_u = i_g \\ i_l = 0 \end{cases} \tag{1}$$

The conducting arm modulates the AC voltage while the other one has all its SMs inserted to minimise the voltage across its DS. So, according to Fig.1, the voltage across the stacks are:

$$\begin{cases} v_{mu} = \dfrac{v_{dc}}{2} - v_v \\ v_{ml} = \hat{V}_m \end{cases} \tag{2}$$

with v_v the AC voltage generated by the converter for a given PQ operating point and $\hat{V}_m$ the maximal voltage producible by a stack.

B. Overlap mode

Both arms conduct the grid current equally distributed through both arms and an overlap current (i_Σ) is flowing through the leg and the DC bus. The expressions of the arm currents in overlap mode are:

$$\begin{cases} i_u = \dfrac{i_g}{2} + i_\Sigma \\ i_l = -\dfrac{i_g}{2} + i_\Sigma \end{cases} \tag{3}$$

AC and DC side equivalent circuits show that the modulated voltage follows the next equations.

$$\begin{cases} v_{mu} = v_\Sigma - v_v \\ v_{ml} = v_\Sigma + v_v \end{cases} \tag{4}$$

with v_Σ the arm DC voltage used to drive i_Σ during the overlap period. In steady-state this voltage is closed to the half of the DC voltage, so, in the following this assumption is considered. The AC currents are controlled on the basis of a power reference coming from external system, while the current i_Σ, at the same time, ensures the energy balance and the active filtering of the DC current. This organisation of the control is illustrated on Fig. 2 where all control layers are clearly stated and the paper topics highlighted.

III. Existing Energy Controls in AAC

The strong coupling between the single phased AC and DC powers caused by the non-overlap mode, makes the stored energy inside AACs naturally unstable in steady-state. This coupling has led to the definition of an ideal operating point where the energy deviation can be strongly limited, called sweet spot. This sweet spot defines that the converter modulation ratio should be around $4/\pi$ (i.e. 1.27) [7]. However, because the grids are dynamic systems, operations at fixed modulation ratio is not possible and it will inevitably lead to a deviation of this energy. To overcome this issue, the use of closed loop control on the converter internal energy proves to be mandatory. Since the advent of the AAC (all overlap lengths included), different methods using the DC power have been explored. Most of them, consist in the exchange of energy between the leg in overlap mode and the DC side as in [12]–[15]. However, they do not comply with the EO-AAC operations, because for each of them, one of the two aforementioned constraints is not fulfilled.

This section analyses these DC power-based energy control techniques to determine which one can be applied to EO-AAC. Three distinct functions are needed: (i) the ability of the chosen energy representation to distribute energy among legs (Horizontal Balancing), (ii) the keep in balance upper and lower stacks (Vertical Balancing) and (iii) to provide a DC current reference for its active filtering.

A. Leg and Total Stored Energy Control

So far, two main approaches have been considered to maintain leg energy levels at their nominal values. The first

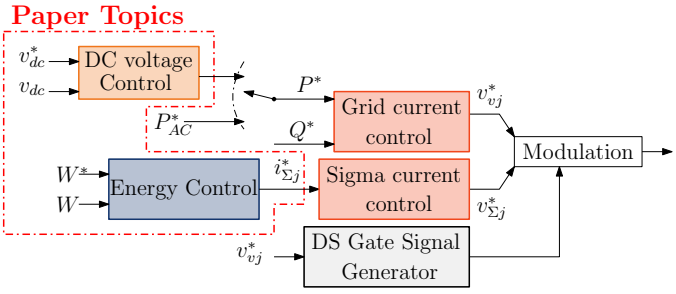

Fig. 2. Overall control scheme of EO-AAC and highlighted paper topics

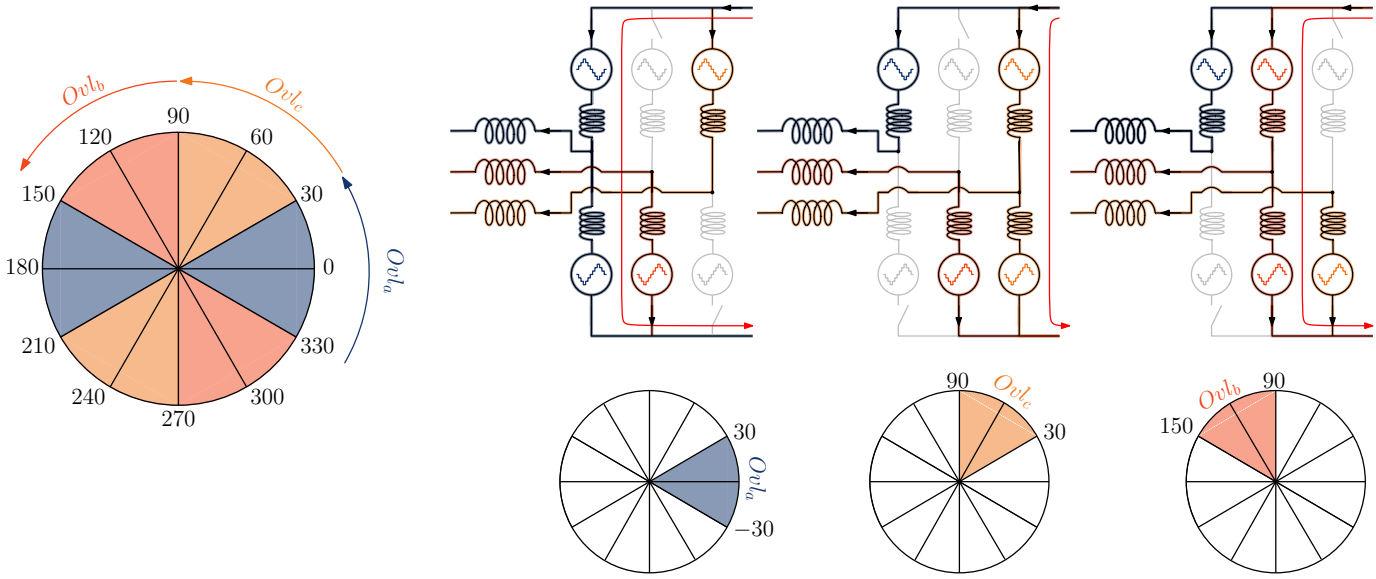

Fig. 3. Example of three different EO-AAC's circuit configurations

one, consists of an adjustment of the overlap period length to modify the power flowing through the converter legs [16], [17]. Because the EO-AAC operates with fixed overlap period this control is therefore not considered. The second approach, which is a also divided into two sub approaches is presented in [12], [14], [15] where each stored energy within the converter legs is regulated in a decoupled way using a DC overlap current, circulating within the leg in overlap mode and the DC bus. By adding the energy stored in the upper and lower stacks of the j phase as

$$\frac{dW_{\Sigma j}}{dt} = \frac{dW_{uj}}{dt} + \frac{dW_{lj}}{dt} \tag{5}$$

and by controlling this combination of stack energies, any deviation within converter legs can be removed thus fulfilling the requirement of Horizontal balancing. Energy controllers essentially operate in average value, so it needs to model the average stored energy ($W_{\Sigma j}$) deviation according to (1)-(4). As detailed in [13] this model can be written as:

$$\left\langle \frac{dW_{\Sigma j}}{dt} \right\rangle_T = V_{dc} i_{\Sigma j} \left(\frac{\theta_{ovl}}{\pi} \right) + P_{acj} \left(\frac{4}{m\pi} \cos\left(\frac{\theta_{ovl}}{2} \right) - 1 \right) \tag{6}$$

with, m the converter modulation ratio and P_{acj} the single phased active power. This single-phased representation highlights that a small amount of DC power depends on i_Σ while the rest is linked to the AC power rectification during the Non-overlap mode thus traducing the aforementioned strong coupling between AC and DC powers. Assuming fixed modulation ratio and overlap period, the only way to compensate the steady-state and transient energy deviation described in (6) lies in the use the overlap current as illustrated on Fig. 2. Using (6) and assuming PI controller the reference of i_Σ (i^*_Σ) can be expressed using the model inversion methodology.

$$\begin{aligned} i^*_{\Sigma j} = & \underbrace{EW_{\Sigma j} \times \left(k_p + \frac{k_i}{s} \right) \left(\frac{\pi}{V_{dc}\theta_{ovl}} \right)}_{\text{constant}} \\ & \underbrace{- P_{acj} \left(\frac{4}{m\pi} \cos\left(\frac{\theta_{ovl}}{2} \right) - 1 \right) \left(\frac{\pi}{V_{dc}\theta_{ovl}} \right)}_{\text{constant}} \end{aligned} \tag{7}$$

with $EW_{\Sigma j}$ the error between reference and measurement. The main limitation of this method (when considering EO-AAC) comes from its utilisation of DC power without taking into account the DC current ripple. This is highlighted in (7) where all terms are constant due to average modelling. It prevents $i^*_{\Sigma j}$ from having an appropriate waveform for active filtering strategy. This control method is therefore limited to the basic AAC topology with shorter overlap angle.

The second approach, presented in [13], focuses on the total stored energy (W_{tot}) deviation. The extended-overlap operation introduces one leg in overlap mode and connected to the DC side at any time. This property of the EO-AAC, makes possible the control of the whole DC power. Thus, obtaining a reference for the DC current is possible. According to [13] this model is given by:

$$\sum_{j=\{a,b,c\}} \frac{dW_{uj}}{dt} + \frac{dW_{lj}}{dt} = \frac{dW_{tot}}{dt} = v_{dc} i_{dc} - p_{ac} \tag{8}$$

As opposed to (6), the total energy deviation can be modelled in instantaneous value as all stack energy oscillations sum to zero. Then, based on (8), the control equation providing a DC current reference (i^*_{dc}) can be written in the same way as (7):

$$i^*_{dc} = \underbrace{\frac{1}{v_{dc}} \left(EW_{tot} \left(k_p + \frac{k_i}{s} \right) + p_{ac} \right)}_{\text{constant}} \tag{9}$$

In (9), under normal conditions, all terms are assumed to be constant allowing to generate ripple free DC current reference.

Then, as only one i_Σ can be controlled at every moment, the calculated DC current reference must be transformed into overlap current reference. Based on circuit analysis it can be shown that:

$$i_{dc} = i_{\Sigma a} + i_{\Sigma b} + i_{\Sigma c} \tag{10}$$

Then, to give i_Σ^* the appropriate waveform enabling active filtering of the DC current, it is required to rest to i_{dc}^* the i_Σ current of the phases in non-overlap mode. For the sake of clarity, the case of leg A in overlap mode is assumed. It means that both legs B and C contributes to the DC current ripple. It results in

$$i_{\Sigma a}^{dcf*} = i_{dc}^* \underbrace{-i_{\Sigma b} - i_{\Sigma c}}_{\text{not constant}} \tag{11}$$

where the index dcf means DC filtering. Using (11) allows to generate an overlap current reference opposing the six pulse ripple in the DC current inherent to the basic AAC topology. Since the example of leg A has been chosen, this equation must be extended to the other cases following the same principle. It can be concluded that this total energy control method is compatible with the EO-AAC topology. The control structure illustrated on Fig. 4 and the resulting arm and DC current waveforms on the first graph of Fig. 5.

These previous derivations have shown the ability of the total energy control to provide active filtering current reference. However, only the sum of the six stacks energy is maintained stable meaning that an even sharing of energy between legs is not achieved. This point could be expected has only one controller is used instead of three. It must be improved.

B. Vertical Balancing Control

This control has been explored [15] and appears to be independent of the overlap period length (i.e. the control is the same for the AAC or EO-AAC). As for MMC, an AC component (i_Σ^{ac}) is required to balance upper and lower stack energies given by

$$\frac{dW_{\Delta j}}{dt} = \frac{dW_{uj}}{dt} - \frac{dW_{lj}}{dt} \tag{12}$$

As for (6), the balance between the upper and the lower stacks have to be modelled in average value as in (13).

$$\left\langle \frac{dW_{\Delta j}}{dt} \right\rangle_T = -2V_{vj} i_{\Sigma j}^{ac} \left(\frac{\theta_{ovl}}{\pi} \right) \tag{13}$$

As pointed out by [15], the AC component has for period the overlap period itself and a square waveform is appropriate. The control outputs RMS values of $i_{\Sigma j}^{ac}$ and an algorithm determines if the square signal should negative or positive first according to the sign of the AC voltage.

The structure of vertical balancing control is shown on Fig. 4 and its impact on DC and arm currents on Fig. 5. The AC component is added to the dcf component of i_Σ and transiently disturbs i_{dc}. With such control, this injection of transient harmonics in the DC current is inevitable as the other legs are not able absorb these harmonics as MMC legs can do [18].

IV. Full Energy Dynamics Control in EO-AAC

The previous section has presented existing stack energy combinations used in the energy management of AACs. It has been demonstrated that, first, only the total energy control can provide a DC current reference necessary for the active filtering and secondly, the vertical balancing control is the same for both the AAC or EO-AAC. Achieving a full energy management to ensure an overall stability of the stacks, requires six feedback controllers but only four are obtained so far. The total energy is only able to maintain an overall energy level but not to equally distribute the energy between legs. In case of transients or asymmetric conditions a difference of energy between them will occur. This difference must be cancelled through the derivation of a Horizontal balancing controller.

A. Modelling of the Energy Difference between Legs

The physical meaning leg energy difference, if the AC grid is assumed to be balanced, is the inequality of DC powers through each leg. To model this inequality, models involving single-phased powers are required. These models have been developed for the original AAC and presented in (6). Combinations of these three models are missing to have a full representation of the energy dynamics in EO-AAC. Two models needs to be defined. So, let us introduce:

$$\begin{cases} \dfrac{dW_{ab}^{\Delta}}{dt} = \dfrac{dW_{\Sigma a}}{dt} - \dfrac{dW_{\Sigma b}}{dt} \\ \dfrac{dW_{ac}^{\Delta}}{dt} = \dfrac{dW_{\Sigma a}}{dt} - \dfrac{dW_{\Sigma c}}{dt} \end{cases} \tag{14}$$

Unlike the total control, to keep balanced leg stored energies it is sufficient to consider their average values. Applying the difference between the legs A and B using (6) yields:

$$\begin{aligned} \left\langle \frac{dW_{ab}^{\Delta}}{dt} \right\rangle_T =& V_{dc} \left(\frac{\theta_{ovl}}{\pi} \right) (i_{\Sigma a} - i_{\Sigma b}) + \\ & (P_{aca} - P_{acb}) \left(\frac{4}{m\pi} \cos\left(\frac{\theta_{ovl}}{2} \right) - 1 \right) \end{aligned} \tag{15}$$

The same equation as (15) is obtained for the difference between the legs A and C. At this stage, assuming balanced AC system makes possible to simplify (15) since all single-phased AC active powers are equal. Moreover, the current i_Σ is in charge of the active filtering and energy management, then, another DC component for the horizontal balancing named i_Σ^Δ is introduced. The overlap current i_Σ is now composed of three distinct components fulfilling different functions taken into account in the model. The AC component (i_Σ^{ac}) interacting with the DC power to balance upper and lower stacks has its impact null in average value, leaving only the dcf and Δ components average values in the model. Thus, a simplified one is obtained:

$$\left\langle \frac{dW_{ab}^{\Delta}}{dt} \right\rangle_T = V_{dc} \left(\frac{\theta_{ovl}}{\pi} \right) (i_{\Sigma a}^{\Delta} - i_{\Sigma b}^{\Delta}) + V_{dc} \left\langle i_{\Sigma a}^{dcf} - i_{\Sigma b}^{dcf} \right\rangle_T \tag{16}$$

The model (16) shows that dcf components are disturbances from the system point of view. It can be shown that dcf

component average value depends on AC and DC currents and the overlap angle such as:

$$\left\langle i_{\Sigma j}^{dcf} \right\rangle_T = I_{dc} - \hat{I}_{gj}\sqrt{3}\sin\left(\frac{\theta_{ovl}}{2}\right)\left(\frac{\theta_{ovl}}{\pi}\right) \tag{17}$$

Introducing (17) within (16) shows that DC currents are simplified leaving terms involving AC side currents. As mentioned above, in this study AC currents are assumed to be balanced, so, all terms related to system disturbances are zero. This leads to the conclusion that in case of balanced AC system, the role of the horizontal control is essentially to assist the total stored energy control during transients by adjusting small amount of DC powers inside each leg. It is therefore obtained:

$$\left\langle \frac{dW_{ab}^{\Delta}}{dt} \right\rangle_T = V_{dc}\left(\frac{\theta_{ovl}}{\pi}\right)\left(i_{\Sigma a}^{\Delta} - i_{\Sigma b}^{\Delta}\right) \tag{18}$$

In comparison with (6) where the three phase stored energies are fully decoupled, this energy representation couple them. A fictitious new coupled basis called 'xyz' is therefore introduced.

$$\begin{cases} \left\langle \frac{dW_{ab}^{\Delta}}{dt} \right\rangle_T = \left\langle \frac{dW_{x}^{\Delta}}{dt} \right\rangle_T = V_{dc}\left(\frac{\theta_{ovl}}{\pi}\right) i_{\Sigma x}^{\Delta} \\ \left\langle \frac{dW_{ac}^{\Delta}}{dt} \right\rangle_T = \left\langle \frac{dW_{y}^{\Delta}}{dt} \right\rangle_T = V_{dc}\left(\frac{\theta_{ovl}}{\pi}\right) i_{\Sigma y}^{\Delta} \\ i_{\Sigma z}^{\Delta} = \sum i_{\Sigma j}^{\Delta} = 0 \end{cases} \tag{19}$$

Since the total stored energy is under control, the sum of all leg stored energy unbalances is zero. Thus, the sum of all Δ components ('z' axis) is zero.

B. Control Design and Reference Decoupling

The controller outputs coupled 'abc' references (xy axis) whereas overlap current controllers are not. Decoupling both controllers output is thus necessary. On the basis of (19) the inverse transformation is presented with the following matrix.

$$\begin{bmatrix} i_{\Sigma a}^{\Delta *} \\ i_{\Sigma b}^{\Delta *} \\ i_{\Sigma c}^{\Delta *} \end{bmatrix} = \begin{bmatrix} 1/3 & 1/3 & 1/3 \\ -2/3 & 1/3 & 1/3 \\ 1/3 & -2/3 & 1/3 \end{bmatrix} \begin{bmatrix} i_{\Sigma x}^{\Delta *} \\ i_{\Sigma y}^{\Delta *} \\ i_{\Sigma z}^{\Delta *} \end{bmatrix} \tag{20}$$

Using (18) and (20) the control structure of the horizontal balancing including reference decoupling is illustrated on Fig. 4. The control is first achieved in the 'xyz' frame, and then (in the purple frame), transformed into instantaneous 'abc' current references.

As the vertical balancing control, the horizontal balancing is independent of the DC current active filtering, and therefore, generates a transient ripple due to its DC power use. The effect of this new component of i_{Σ} is shown on the second graph of Fig. 5. As visible, the Δ component adds a DC offset around the DC current obtained with the active filtering strategy.

C. Validation With EMT Simulation

To validate models and controllers, this section presents EMT simulation results using EMTP-RV simulation software whose main parameters are given in Table I.

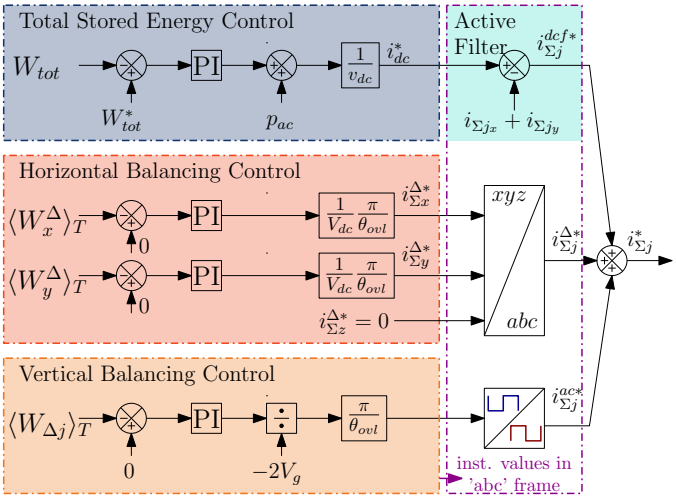

Fig. 4. EO-AAC's energy control structures

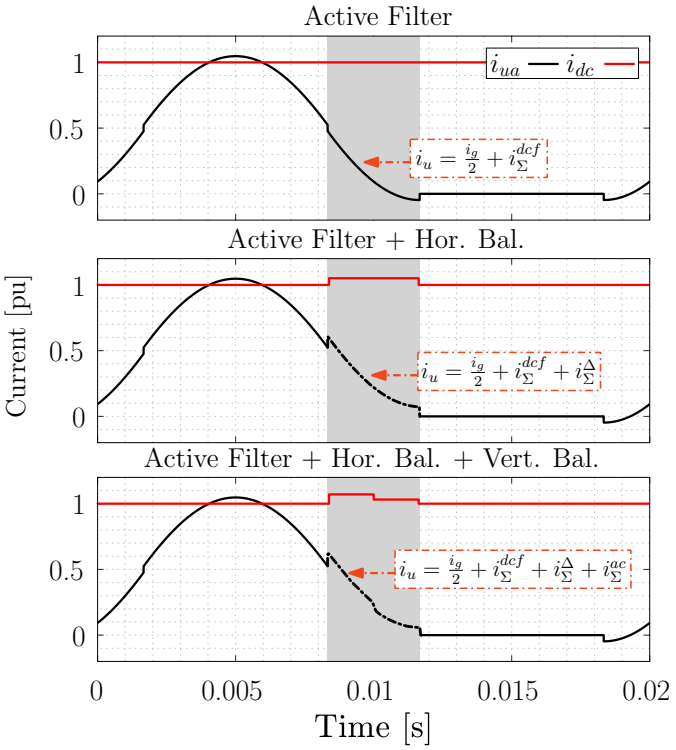

Fig. 5. Illustration of the DC power utilisation for energy balancing during one overlap period including the impact on DC current

The overall system can be excited by modifying the different control references highlighted on Fig. 2. The first one is the energy reference; however, unless energy controller response times are tested, there are no reasons to use this one. The second one is the DC voltage reference, which is fixed by the HVDC system. It remains the power reference coming from external system requirements (AC and DC grids) which is more likely to be varied in practice. So, it is chosen to act on this system input. The simulated scenario is the following one:

- At 0.1s a power ramp of - 1 GW / 100 ms
- At 0.35s a power step of 1 GW

TABLE I
PARAMETERS OF EO-AAC

Parameter	Name	Value
Rated Power	S	1.044 GVA
DC Voltage	V_{dc}	640 kV
Grid Voltage (RMS-LL)	U_g	500 kV
Embedded Stored Energy	H_c	15 kJ/MVA
Total Energy Control response time	t_{Wtot}	50 ms
Total Energy Control damping ratio	ζ_{Wtot}	0.707
Balancing Controls response time	t_{Wbal}	100 ms
Balancing Controls damping ratio	ζ_{Wbal}	0.707

- Finally, at 0.5s a power step of 1 GW

In a first simulation, the need of a full energy management is highlighted by showing results without horizontal and vertical balancing controllers. Then a second simulation is performed using the proposed control structure. In practice, it must be noted that active power steps may not occur while power ramping is more likely. Nonetheless, validating the behaviour of the converter under such severe events give a good performance indicator about the proposed controls.

First of all, the results of the proposed simulation scenario without horizontal and vertical balancing are shown on Fig. 6. Starting the simulation by power ramping illustrates the lack of information that may give such events. Because the power variation is so smooth, the energy tends to be well distributed between all stacks. During and after the power raping, there is almost no energy deviations regarding all Δ energy variables presented on the second graph. However, at the moment when the converter get stressed by the power steps, the open-loop control clearly shows its limitation since the energy between stacks is no more properly distributed. To avoid this issue, the use of a full energy management is necessary to keep all stacks closed to their nominal value in order to guarantee arm voltage availability.

Fig. 7 introduces the proposed energy controllers using Fig. 4. During the power ramping event, there are no real differences between this result and the one in open-loop control since this event does not sufficiently stress the converter. However, at power step instances, the energy within stacks deviate and thanks to the energy management they go back to their initial states. The total stored energy control increases the DC power reference to ensure equality between both side powers while, balancing controls evenly distribute the energy inside each stack with respect to their slower dynamics. As expected and shown on Fig. 5 the transient ripple on the DC current is visible. In around 200 ms, the energy inside all stacks is stable and closed to their nominal values and the DC current smooth.

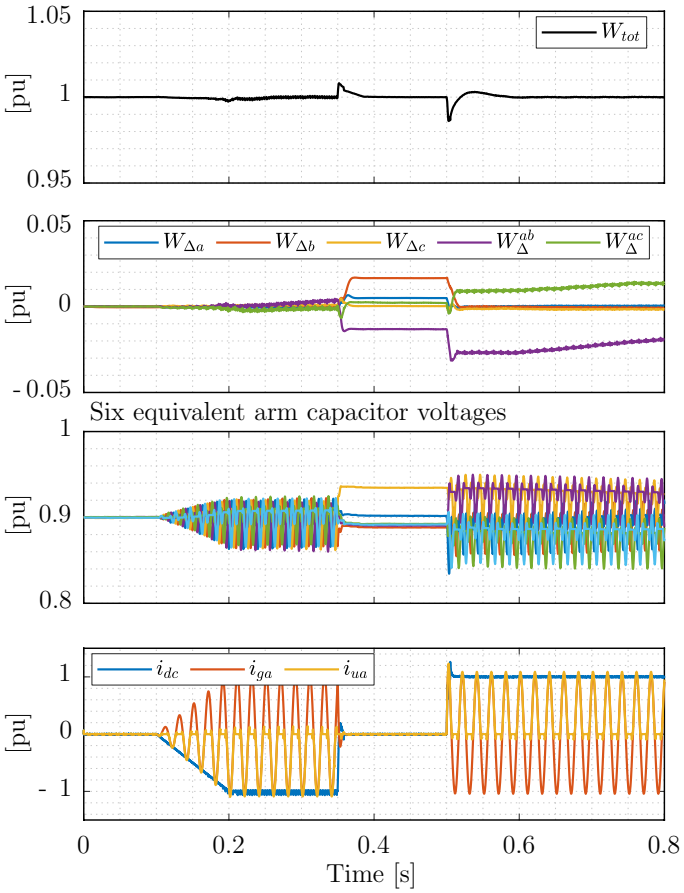

Fig. 6. Dynamic simulation results without Horizontal and Vertical balancing as in [13]

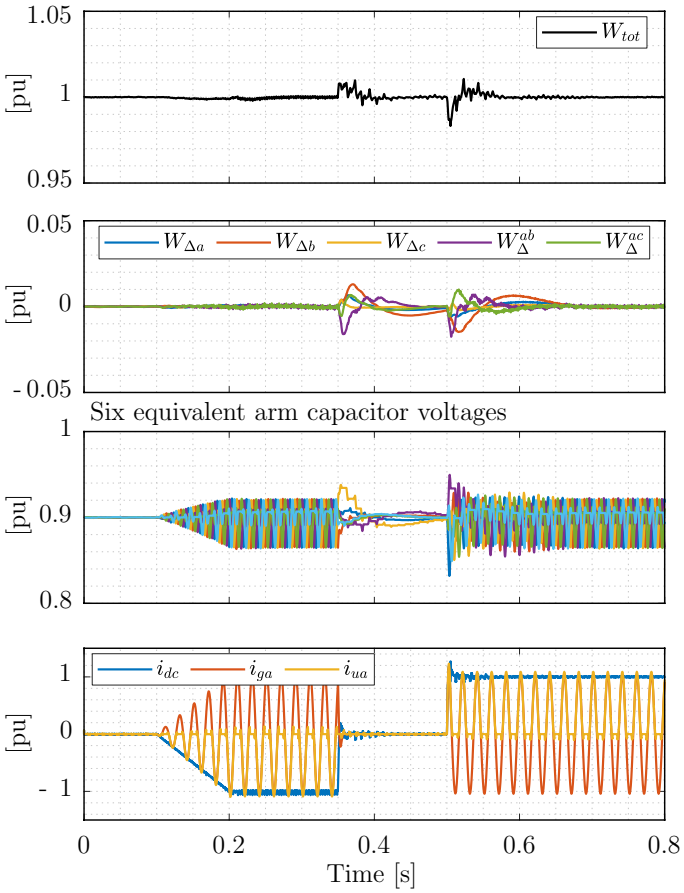

Fig. 7. Dynamic simulation results with the proposed energy controllers

To go further, from the results obtained on Fig. 7, the transient behaviour of the EO-AAC stored energy can be discussed to clarify one of its essential dynamic property. In contrast to the MMC, the EO-AAC has only two stacks in overlap mode and able to maintain the power balance. By controlling the total energy deviation in instantaneous value and with faster dynamics than balancing controls, this single converter leg is forced to, temporarily, behave as three legs. This point was implicitly described by (11) where the reference of the overlap current (i^*_Σ) is calculated based on the DC current reference which directly derives from the deviation of W_{tot}. Thereby, the power required to keep the total energy stable, is temporarily furnished or absorbed by the phase-leg in overlap mode.

Thereby, the behaviour of the EO-AAC leg in overlap mode, allows to interface, virtually, the AC and DC powers through an equivalent storage devices equals to six times the equivalent stack capacitors (i.e. C_{tot} in Fig. 1). Such dynamic behaviour, was already observed for MMC in [19] where the equivalent capacitor seen by the DC grid is six time the equivalent stack capacitors. This observation allows to conclude that, an EO-AAC embedding a full energy management has the same controllability and equivalent dynamics as a MMC. To demonstrate this similar behaviour, the following section investigates the application of a MMC DC voltage control concept to the EO-AAC.

V. DC Voltage Control with EO-AAC

DC voltage control ensures stable operation of HVDC system. However, when considering DC cables, the DC voltage is no longer stiff and highly deviates with transient on DC power due to low internally stored energy. For this reason, the use of modular converters internal energy to increase the effective capacitance of DC cables has been investigated in MMC literature [20]. Till now, the limited energy control of the AAC prevented from applying this principle but now, thanks to the proposed control, it is possible to make a strong relation between the level of internal energy and the DC bus voltage.

A. Modelling DC Voltage Dynamics under Virtual Capacitor Control

To represent DC voltage dynamics, for the purpose of control design, focusing on cable stored energy is enough. As it is mostly stored in the electrostatic form, it is chosen to only consider the cable capacitance (C_{dc}). Based on a power balance at both cable ends yields:

$$\frac{1}{2}C_{dc}\frac{dv_{dc}^2}{dt} = -p_{dc1} - p_{dc2} \tag{21}$$

where p_{dc1} and p_{dc2} are the DC powers of station 1 and station 2 respectively. It should be noted that this model is obtained based on DC powers (at each converter terminals) flowing inside the converters as in Fig.1 (i.e. from DC to AC sides). When modular type converters are connected to the grid, DC powers in (21) can be replaced according to (8):

$$\frac{1}{2}C_{dc}\frac{dv_{dc}^2}{dt} + \frac{dW_{tot1}}{dt} + \frac{dW_{tot2}}{dt} = -p_{ac1} - p_{ac2} \tag{22}$$

(22) shows that both AC grids, could be interfaced through one single DC dynamics (the left-hand term) if converter total energies are managed according to the DC voltage level. As demonstrated above, the EO-AAC is able to maintain its total energy at a desired constant value through one single leg in overlap mode using (11). Now, it is proposed to validate this property with a variable energy reference.

To do so, the following content is based on the assumption that all stacks are replaced by average arm models shown on Fig. 1. It involves the sum of the SM capacitor voltages (v_{Ctot}) and the aggregated SM capacitance C_{tot}. In MMC literature, it was shown that such model provides sufficient information for system level studies.

In operation, the energy inside all stacks is oscillating at different frequencies and angles. As shown on Fig. 7, the active filtering control makes all these oscillations to sum to zero leaving the total energy harmonic free. Defining $\langle v_{Ctot}\rangle$ the average value of the six v_{Ctot} gives the expression of the total stored energy:

$$W_{tot} = 3C_{tot}\langle v_{Ctot}\rangle^2 \tag{23}$$

EO-AAC stacks are designed to be able to generate enough voltage to oppose the grid voltage in case of DC-fault. This means that, unlike HB-MMC, V_{Ctot0} the nominal value of v_{Ctot} is different from V_{dc0} the nominal DC voltage enforcing the use of k_m defined as:

$$k_m = \frac{V_{Ctot0}}{V_{dc0}} \tag{24}$$

Using k_m allows to express the nominal total stored energy (W_{tot0}) with respect to V_{dc0}.

$$W_{tot0} = 3C_{tot}k_m^2V_{dc0}^2 \tag{25}$$

A first solution in the total energy control consist in maintaining the energy at a constant reference value W^*_{tot0} assumed to be equal to the nominal energy as achieved in Fig. 7. Thus,

$$W^*_{tot} = W^*_{tot0} = W_{tot0} \tag{26}$$

A second solution lies in adjusting the energy with respect to the instantaneous value of v_{dc} deviation. This is the concept of virtual capacitor control [20]. The expression of total energy reference with virtual capacitor control is given as follows:

$$W^*_{tot} = W^*_{tot0} + \Delta W^*_{tot} \tag{27}$$

with,

$$\Delta W^*_{tot} = 3k_{vc}k_m^2C_{tot}\left(v_{dc}^2 - V_{dc0}^2\right) \tag{28}$$

and k_{vc} the virtual capacitor coefficient allowing to modulate the action of the converter to support the DC voltage. As shown in (28), the energy reference is now modified according to the DC voltage deviation and the value of k_{vc}. Under the assumption that $W_{tot} \simeq W^*_{tot}$ yields:

$$\frac{1}{2}\left(C_{dc} + \sum_{i=1}^{n} 6k_{vci}k_{mi}^2C_{toti}\right)\frac{dv_{dc}^2}{dt} = \sum_{i=1}^{n} -p_{aci} \tag{29}$$

with i for the i^{th} station. Applying the virtual capacitor concept to HB-MMC is almost straightforward as all stack energies continuously interface the AC and DC powers. This

concept can also be applied to the EO-AAC as long as the converter is able to control W_{tot} and to maintain an acceptable level of energy inside all the stacks. This is achieved thanks to the horizontal and vertical balancing which make sure that no stacks support too much charge or discharge. Thus, the only difference between MMC and EO-AAC based virtual capacitor control would be the stack sizing, i.e. embedded stored energy (15 kJ/MVA for the EO-AAC and 40 kJ/MVA for the MMC).

B. Extension to Any Topology Able to Control W_{tot}

The model (29) suffers of a lack of generality. Indeed, in (29) stack voltage sizing is present at the same time in k_m and C_{tot} preventing from a comprehensive description of the DC voltage dynamics after including virtual capacitor control. Thus, to be as generic as possible, the following equations extend the virtual capacitor main equations to any topology able to control W_{tot} without the influence of stack sizing. As mentioned above, C_{tot} depends on the number of SMs (i.e. C_{sm}/N_{sm}) but also from the stored energy requirement (H_C in kJ/MVA). The expression of H_C is recalled hereafter:

$$H_C = \frac{3C_{tot}V_{Ctot0}^2}{S_n} \rightarrow C_{tot} = \frac{H_C S_n}{3k_m^2 V_{dc0}^2} \tag{30}$$

With S_n the rated power. Introducing (30) into (27) yields

$$W_{tot}^* = k_{vc}\frac{H_C S_n}{V_{dc0}^2}\left(v_{dc}^2 - V_{dc0}^2\right) + W_{tot0}^* \tag{31}$$

As shown in (31), the coefficient k_m is removed highlighting the only quantity that matters in the virtual capacitor control: H_C that may be assimilated as an inertia from the grid point of view. This allows to provide a comprehensive determination of the effective DC bus stored energy. Thus, the generic model of the DC voltage dynamics, for HVDC link or MTDC system and for any converter topology (AC/DC and DC/DC) able to control their total energy (i.e. Difference between input and output powers) is:

$$\frac{1}{2}\left(C_{dc} + \frac{\sum_{i=1}^{n} k_{vci}H_{Ci}S_{ni}}{V_{dc0}^2}\right)\frac{dv_{dc}^2}{dt} = \sum_{i=1}^{n} -P_{aci} \tag{32}$$

VI. HVDC Link Simulation Results

In this section converter models are the same as Section IV. The DC cable is represented by a wideband model provided by the EMTP-RV library and its length is 300 km. The response time of the DC voltage is set to 70 ms and the control scheme of the converter including DC voltage control is illustrated on Fig. 8. The energy reference can be constant or coupled to the DC voltage. Both cases are presented.

In order to validate the use of virtual capacitor control with EO-AAC, it is chosen to disturb converters and the HVDC link by using the active power which is involved in the converter energy model as well as in the DC voltage one. The first event of this simulation is a power reversal (-1 GW to 1 GW) achieved in 100 ms in order to present the behaviour of the converter under DC voltage drops. Then, as every modular converters, since the number of SMs per stack is limited the EO-AAC is not able to deal with high DC over-voltage. To

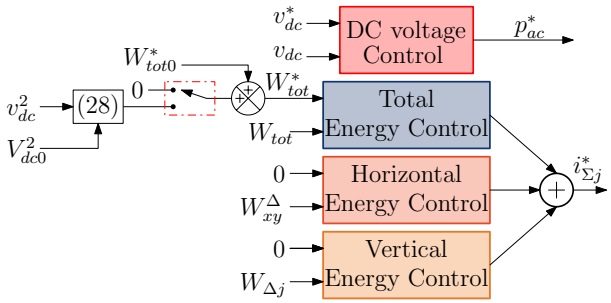

Fig. 8. EO-AAC DC Voltage and Energy controllers scheme representation

simulate this over-voltage situation, after the power reversal a power outage in the side of the EO-AAC in power control mode (i.e. EO-AAC 2) is simulated. The interruption of the active power through the HVDC link create an excess of energy in DC cables resulting in a fast increasing of the voltage. In summary:

- At 0.25 second a power reversal is applied to EO-AAC 2 AC power reference (-1 GW to 1 GW).
- At 0.5 second EO-AAC 2 has to stop exchanging active power, its reference is set to 0.

A. Case 1 : Converters without virtual capacitor control

In this case, both converters manage their internal energies using (26). The DC voltage dynamics only relies on cable stored energy, so approximately 13 kJ/MW (DC cable capacitance is about 0.2 μF per km). The obtained results are illustrated on Fig. 9. Until 0.25 second all quantities are stable and under control. Then, after 0.25 second the active power flow is reversed creating a deficit of energy in cables leading to a decreasing of the DC voltage. This decreasing reaches 0.8 p.u at EO-AAC 1 terminals and slightly less at the other cable end due to stored energy in cable inductance. Nonetheless, every internal dynamics are kept under control, the total energy is maintained constant and the DC current as well despite 20% of DC voltage deviation. At 0.5 second, EO-AAC 2 has to stop the power flow. Quickly, due to low dynamics of voltage control v_{dc} increases, converters run out of available SM to deal with the over-voltage situation and lose controllability.

The first consequence is a bad blocking of the DSs when they are supposed to be turned off leaving diodes conducting and creating an uncontrollable current path. This phenomenon is visible on the arm and DC currents where high current spikes are visible. Over-current protections are activated requiring the AC breakers to be opened since the power is already zero. The opening occurs at the moment noted ① on Fig. 9. Once the arm currents are zero and the DC voltage stabilised, AC breakers are reset on ② allowing the station on charge of the DC voltage control to inject power in its AC side to bring v_{dc} to its nominal value. Finally, in ③ the energy controllers return in normal operation in order to bring all stack energies to their nominal values.

B. Case 2 : Converters with virtual capacitor control

In this second case, both converters have their energies coupled with the DC bus as in (27), and both k_{vc} are equal

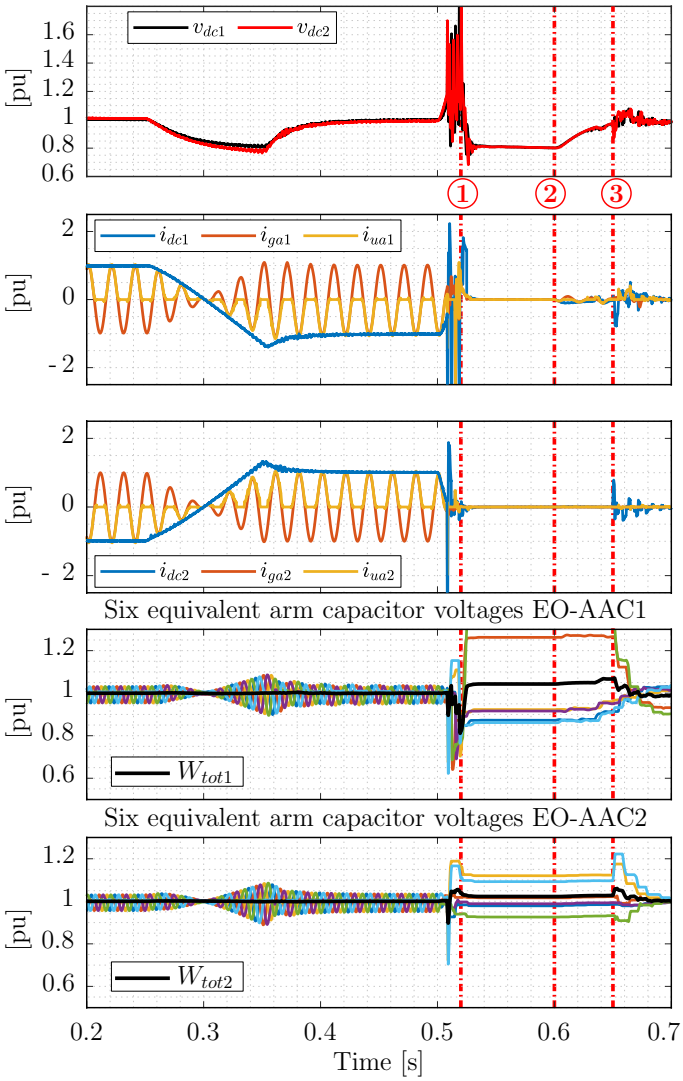

Fig. 9. Case 1: HVDC Link simulation results without DC voltage support

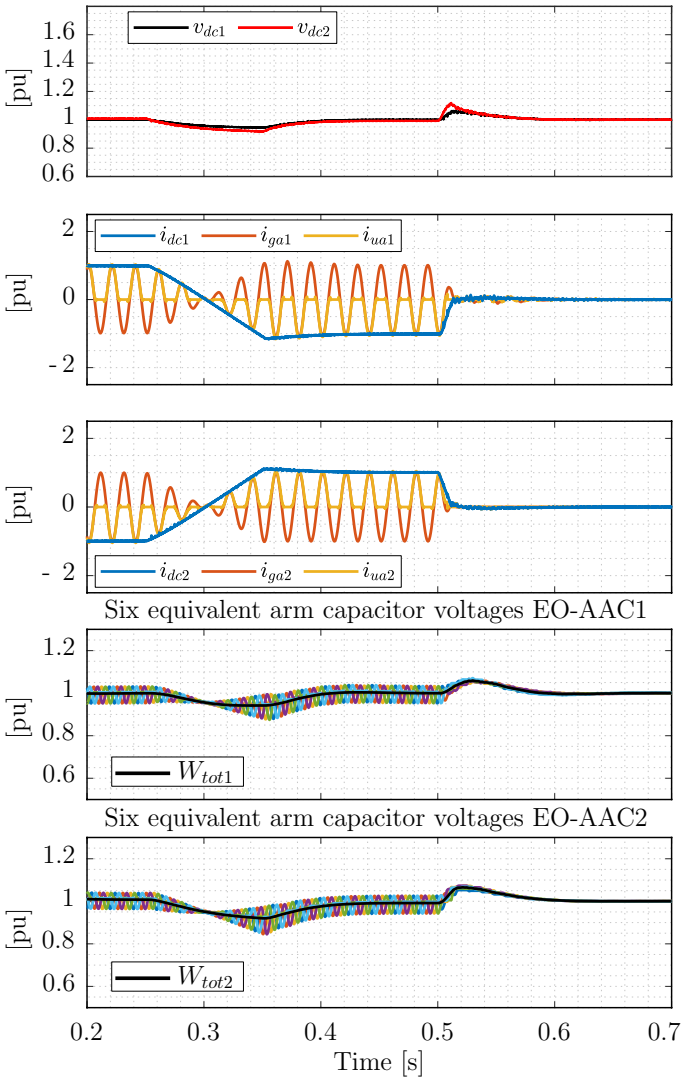

Fig. 10. Case 2: HVDC link simulation results with DC voltage support

to 1. The EO-AACs embed 15 kJ/MVA of stored energy, making the effective DC side stored energy about 43 kJ/MW under the assumption that S_n is closed to nominal active power P_n (2×15 kJ/MW for EO-AACs + 13 kJ/MW for DC cables). Results are presented on Fig. 10. Thanks to the use of the converters internal energies, the capacity of the DC link to withstand DC power variation has increased. Indeed, regarding the first event which is the power reversal, the gain observed is above 10% less of DC voltage deviation. At EO-AAC 1 terminals v_{dc1} drops up to 0.95 p.u while EO-AAC 2 sees about 0.92 p.u. This first result shows the interest of using such control to support HVDC system and also the ability of the converter leg in overlap mode to behave as if there were 6 stacks connected to the DC side without major difficulties. It is also observed that thanks to the horizontal and vertical balancing, the stacks are kept balanced during every transients. Then, the second observation is the removal of the instability at the power interruption instance. The fact that both converter energies follow the DC voltage makes possible to avoid arm voltage unavailability observed in the previous case. The controllability of the converters is therefore extended. As visible on the first graph, DC voltage at each terminal is now kept closer to the nominal value, or at least, in a range that converters can handle. This is made possible by the two EO-AACs absorbing the excess energy inside DC cable and therefore reducing peak value of v_{dc}. The excess of energy is around 1.1 p.u for the EO-AAC in power control mode which has to support the highest DC voltage value due to the inductance of cables.

VII. Conclusion

The study of a full energy management inside the Extended Overlap Alternate Arm Converter, a modular type converter, has been presented in this paper and revealed that the energy level in all six stacks can be fully controlled using different current-based control methods jointly functioning. The management of all stack energies is performed through four essential functions: the total energy control which decouple the AC and DC power thanks to the Extended Overlap operation, the active filtering function based on the DC current reference

provided by the total energy control allowing to generate arm current references with harmonic compensation and finally, the horizontal and vertical balancing which ensure the equal distribution of energy between legs and arms. This full energy management has been validated through detailed EMT simulations and under severe active power step events. From these results, it is demonstrated that through only two stacks in overlap mode the EO-AAC, despite its inherent discontinuous internal behaviour, is able to provide equivalent dynamics to MMC which uses six stacks to decouple the AC and DC powers. In other words, these two stacks in overlap mode, ensure the power decoupling by acting as if they were six physical stacks connected to DC side. On the basis of this common dynamic property between MMC and EO-AAC, it is also demonstrated that as long as the converter is able to maintain the control of its total energy and an acceptable level of energy inside each stack, the application of the so-called virtual capacitor, a concept so far specific to MMC, is possible.

REFERENCES

[1] A. Lesnicar and R. Marquardt, "An innovative modular multilevel converter topology suitable for a wide power range," in *2003 IEEE Bologna PowerTech - Conference Proceedings*, vol. 3. IEEE, jun 2003, pp. 272–277.

[2] C. C. Davidson and D. R. Trainer, "Innovative concepts for hybrid Multi-Level converters for HVDC power transmission," in *IET Conference Publications*, vol. 2010, no. 570 CP, oct 2010, pp. O51–O51.

[3] C. Oates and K. Dyke, "The controlled transition bridge," *2015 17th European Conference on Power Electronics and Applications, EPE-ECCE Europe 2015*, 2015.

[4] M. B. Ghat and A. Shukla, "A New H-Bridge Hybrid Modular Converter (HBHMC) for HVDC Application: Operating Modes, Control, and Voltage Balancing," *IEEE Transactions on Power Electronics*, vol. 33, no. 8, pp. 6537–6554, aug 2018.

[5] C. Martinez, A. Costabeber, E. Amankwah, D. Trainer, and J. Clare, "A decoupled energy control strategy for the Series Bridge Converter (SBC) for HVDC applications," *Proceedings - 2017 IEEE Southern Power Electronics Conference, SPEC 2017*, vol. 2018-Janua, pp. 1–6, 2018.

[6] J. Yang, Z. He, J. Ke, and M. Xie, "A New Hybrid Multilevel DC-AC Converter with Reduced Energy Storage Requirement and Power Losses for HVDC Applications," *IEEE Transactions on Power Electronics*, vol. 34, no. 3, pp. 2082–2096, 2019.

[7] M. M. Merlin, T. C. Green, P. D. Mitcheson, D. R. Trainer, R. Critchley, W. Crookes, and F. Hassan, "The alternate arm converter: A new hybrid multilevel converter with DC-fault blocking capability," *IEEE Transactions on Power Delivery*, vol. 29, no. 1, pp. 310–317, 2014.

[8] P. Bakas, K. Ilves, S. Norrga, L. Harnefors, and H. P. Nee, "Hybrid alternate-common-arm converter with director thyristors - Impact of commutation time on the active-power capability," *2019 21st European Conference on Power Electronics and Applications, EPE 2019 ECCE Europe*, pp. P.1–P.11, 2019.

[9] J. Chivite-Zabalza, D. R. Trainer, J. C. Nicholls, and C. C. Davidson, "Balancing Algorithm for a Self-Powered High-Voltage Switch Using Series-Connected IGBTs for HVDC Applications," *IEEE Transactions on Power Electronics*, vol. 34, no. 9, pp. 8481–8490, 2019.

[10] M. M. Merlin and T. C. Green, "Cell capacitor sizing in multilevel converters: Cases of the modular multilevel converter and alternate arm converter," *IET Power Electronics*, vol. 8, no. 3, pp. 350–360, 2015.

[11] M. M. C. Merlin, D. Soto-Sanchez, P. D. Judge, G. Chaffey, P. Clemow, T. C. Green, D. R. Trainer, and K. J. Dyke, "The extended overlap alternate arm converter: A voltage-source converter with DC fault ride-through capability and a compact design," *IEEE Transactions on Power Electronics*, vol. 33, no. 5, pp. 3898–3910, 2018.

[12] H. R. Wickramasinghe, G. Konstantinou, and J. Pou, "Gradient-Based Energy Balancing and Current Control for Alternate Arm Converters," *IEEE Transactions on Power Delivery*, vol. 33, no. 3, pp. 1459–1468, 2018.

[13] P. Vermeersch, F. Gruson, M. M. Merlin, X. Guillaud, and P. Egrot, "A stored energy control based active DC filter for the alternate arm converter with an extended overlap period," in *2019 21st European Conference on Power Electronics and Applications, EPE 2019 ECCE Europe*. IEEE, sep 2019, pp. P.1–P.10.

[14] S. Liu, M. Saeedifard, and X. Wang, "Zero-current switching control of the alternate arm HVdc converter station with an extended overlap period," *IEEE Transactions on Industrial Electronics*, vol. 66, no. 3, pp. 2355–2365, 2019.

[15] P. Vermeersch, F. Gruson, X. Guillaud, M. M. Merlin, and P. Egrot, "Energy and director switches commutation controls for the alternate arm converter," *Mathematics and Computers in Simulation*, vol. 158, pp. 490–505, dec 2018.

[16] Y. Y. Leow and C. A. Ooi, "Arm energy balancing control in AACs: A comparative analysis," *IET Power Electronics*, vol. 13, no. 6, pp. 1113–1128, 2020.

[17] S. Howell, H. Wang, and S. Filizadeh, "Alternate arm modular multilevel converter energy balancing via overlap onset control," *The Journal of Engineering*, vol. 2019, no. 16, pp. 1649–1655, oct 2019.

[18] P. Münch, D. Görges, M. Izák, and S. Liu, "Integrated current control, energy control and energy balancing of modular multilevel converters," in *IECON Proceedings (Industrial Electronics Conference)*, 2010, pp. 150–155.

[19] L. Harnefors, A. Antonopoulos, S. Norrga, L. Angquist, and H. P. Nee, "Dynamic analysis of modular multilevel converters," *IEEE Transactions on Industrial Electronics*, vol. 60, no. 7, pp. 2526–2537, 2013.

[20] K. Shinoda, A. Benchaib, J. Dai, and X. Guillaud, "Virtual Capacitor Control: Mitigation of DC Voltage Fluctuations in MMC-Based HVdc Systems," *IEEE Transactions on Power Delivery*, vol. 33, no. 1, pp. 455–465, feb 2018.

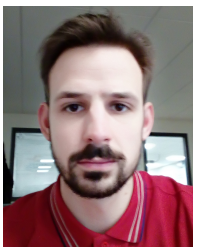

Pierre Vermeersch received the M.S.c degree in Electrical Engineering for Suistainable Development from the Université de Lille, France in 2017. Since 2018 he is working toward the PhD degree on design and control of grid connected modular type converters at Ecole Centrale de Lille, France. His reseach interests include power electronics and HVDC systems.

Francois Gruson (M'14) received the Ph.D. degree in electrical engineering from the Ecole Centrale de Lille, Lille, in 2010. Since 2011, he has been working as Associate Professor at Arts and Metiers ParisTech in the Laboratoire d'Electrotechnique et d'Electronique de Puissance of Lille (L2EP), Lille, France. His research interests include power electronic converter and power quality for distribution and transmission grid applications and especially for HVDC transmission grid.

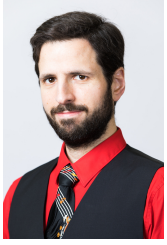

Michael M.C. Merlin Michael M. C. Merlin (M'12) received the electrical engineering degree from the Ecole National Superieur de l'Electronique et de ses Applications (ENSEA), Cergy, France, in 2008 and the M.Sc. degree in control systems then the Ph.D. degree in electrical engineering from Imperial College, London, U.K. in 2008 and 2013 respectively. He became a Lecturer at the University of Edinburgh in 2017. His main research interest are design, optimization and control of power converters, more specifically of the modular types which use stacks of sub-modules to achieve high power efficiency and waveform quality.

Xavier Guillaud (M'04) has been professor in L2EP - Lille since 2002. First, he worked on the modeling and control of power electronic systems. Then, he studied the integration of distributed generation and especially renewable energy in power systems. Nowadays, he is studying the high voltage power electronic converters in transmission system. He is leading the development of an experimental facility composed of actual power electronic converters interacting with virtual grids modelled in real-time simulator. He is involved on several projects about power electronic on the grid within European projects and different projects with French companies. He is member of the Technical Program Committee of Power System Computation Conference (PSCC) and associated editor of Sustainable Energy, Grids and Networks (SEGAN).

Philippe Egrot Philippe Egrot (born in 1964, France) graduated from INPG, France, began his career at MATRA Telecom, Telecommunications Department, in 1986. After joining ERDF the French DSO (Enedis today) in 1989, he reached EDF Research and Development Division, as a mechanical engineer to work on tests and modeling on overhead line equipments and lattice towers. Following this, he managed several laboratories, High Voltage and Mechanics Laboratory in 2000, High Power Laboratory in 2003. From 2008, he managed Research Projects on HVDC systems and Supergrids issues covering high voltage cables and overhead lines, power electronics and components, DC circuit breakers, offshore platforms for renewable energy. Today he is a Senior research Engineer focusing on planetary Supergrids question and grids technologies.